Electronic Supplementary Material (ESI) for Journal of Materials Chemistry A.

Supporting Information for

Thermostable carbon-supported subnanometer-sized (< 1 nm) Pt clusters for hydrogen evolution reaction

Jing-Fang Huang, *[a] Ruo-Hua Zeng,[a] and Jeng-Lung Chen[b]

[a] Department of Chemistry, National Chung Hsing University, Taichung 402, Taiwan

[b] National Synchrotron Radiation Research Center, Science-Based Industrial Park, Hsinchu 30076, Taiwan

Correspondence to: jfh@dragon.nchu.edu.tw

This PDF file includes:

S-1. Tannic acid adsorption on the carbon surface

The area of a single molecule of TA

The radius of a TA molecule was determined by measuring the length from its center (A) to one of the end hydroxyl groups (B) (Fig. S1). The A-B length was measured to be ~1.28 nm. Thus, the area of a single molecule of TA (A_{TA}) is calculated as follows.[1]

$A_{TA} = [2 \times (1.28 \times 10^{-9}\ m)]^2 = \sim 7 \times 10^{-18}\ m^2$

Coverage of TA on GCE (one monolayer)

Surface area of GCE/A_{TA} = $7 \times 10^{-6}\ m^2 / 7 \times 10^{-18}\ m^2$

= $\sim 1 \times 10^{12}$ molecules/GCE

= $\sim 1.66 \times 10^{-12}$ moles/GCE

Coverage of TA on XC-72 (one monolayer)

A_{BET} of XC-72/A_{TA} = $130\ m^2/gC / 7 \times 10^{-18}\ m^2$

= 1.86×10^{19} ($\sim 2 \times 10^{19}$) molecules/gC

Coverage of TA on XC-72/GCE (one monolayer)

A carbon loading of 9.52 μg cm^{-2} was drop-dried on a GCE (0.07 cm^2)

- 0.67 μg XC-72 on the GCE and the A_{BET} of XC-72 is approximately 130 $m^2\ g^{-1}$
- Total surface area of XC-72 on the GCE (A_c) = $6.7 \times 10^{-7} \times 130 = 8.7 \times 10^{-5}\ m^2$

Coverage of TA on XC-72/GCE (one monolayer):

$A_c/A_{TA} = 8.7 \times 10^{-5}\ m^2 / 7 \times 10^{-18}\ m^2$

= $\sim 1.24 \times 10^{13}$ molecules/GCE

= $\sim 2.06 \times 10^{-11}$ moles/GCE

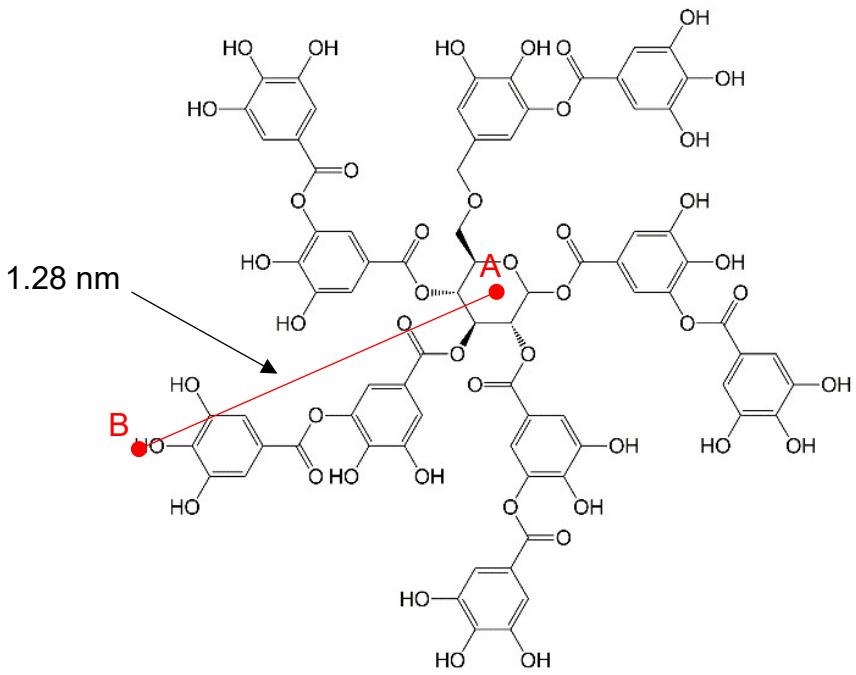

Fig. S1 molecule structure of TA

S-2. $PtCl_4^{2-}$ monolayer adsorption on TA_i/C

The TA adsorption (TA_{ad}) on carbon (TA/C) was monitored by CV of TA/C/GCE in a 1.0 M KOH aqueous solution (KOH_{aq}). As shown in Figure S2, CVs reveal broad TA oxidation waves from 0.85 V to 1.6 V vs. RHE assigned for the oxidation of TA to TA-quinone through the $2e^-/2H^+$ process.[1] The integrated charges of these waves determine the amount of TA_{ad}. Based on an estimated effective radius of 1.28 nm for the TA molecule (Fig. S1), corresponding to the BET surface area (A_{BET}) of XC-72 (130 m^2/g), the TA_{ad} in one monolayer is estimated to be ~2×10^{19} molecules per gram of C. Saturated TA_{ad} on XC-72 (TA_m/C) reached ~36 molecule layers. TA_{ad} sharply decreased from 36 molecule layers to only ~4 molecule layers (8.5×10^{19} molecules per gram of C) on TA_i/C from TA_m/C incubated in 1.0 M KOH_{aq} (pH ~13) for 5 min. $PtCl_4^{2-}$is a Pt_c precursor adsorbed on TA_i/C ($PtCl_4^{2-}/TA_i/C$) dispersed in neutral di-water. After $PtCl_4^{2-}/TA_i/C$ precipitation was complete (~2 h), the reduction in absorbance on $\lambda_{216\,nm}$ (ligand to metal charge transfer) in the UV-Vis spectrum of $PtCl_4^{2-}$ upper aqueous solution (Figure S3) determined the amount of $PtCl_4^{2-}$ on TA_i/C ($PtCl_4^{2-}{}_{ad}$). $PtCl_4^{2-}{}_{ad}$ on TA_i/C is ~4.1×10^{19} ions per gram of C, which is lower than $PtCl_4^{2-}{}_{ad}$ on naked C (~1.6×10^{20} ions per gram of carbon). The atomic ratio of Pt to TA was ~2 for TA_i/C. TA inhibits $PtCl_4^{2-}$ non-specifically physical adsorption on carbon. The H-bonding between $PtCl_4^{2-}$ and -OH of TA mainly controlled $PtCl_4^{2-}{}_{ad}$ on TA_i/C.

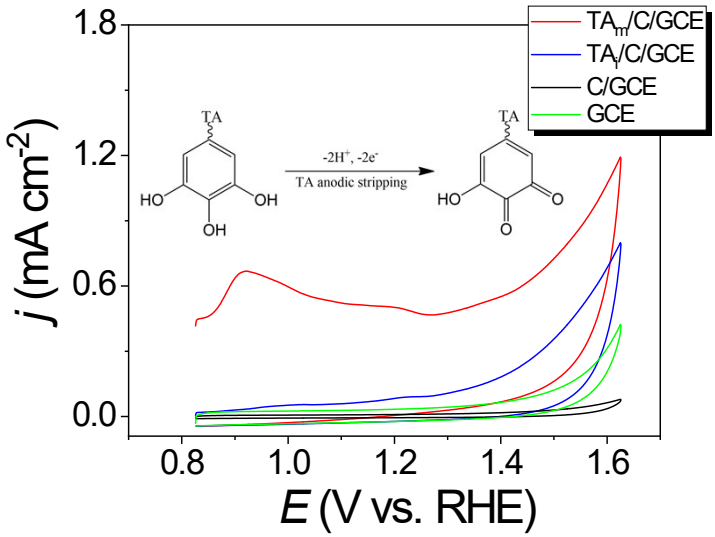

Fig. S2 CVs of $TA_m/C/GCE$, $TA_i/C/GCE$, C/GCE, and GCE were recorded in 1.0 M KOH_{aq} with a scan rate of 50 mV s^{-1}. The inset is a $2e^-/2H^+$ process for the oxidation of TA to TA-quinone.

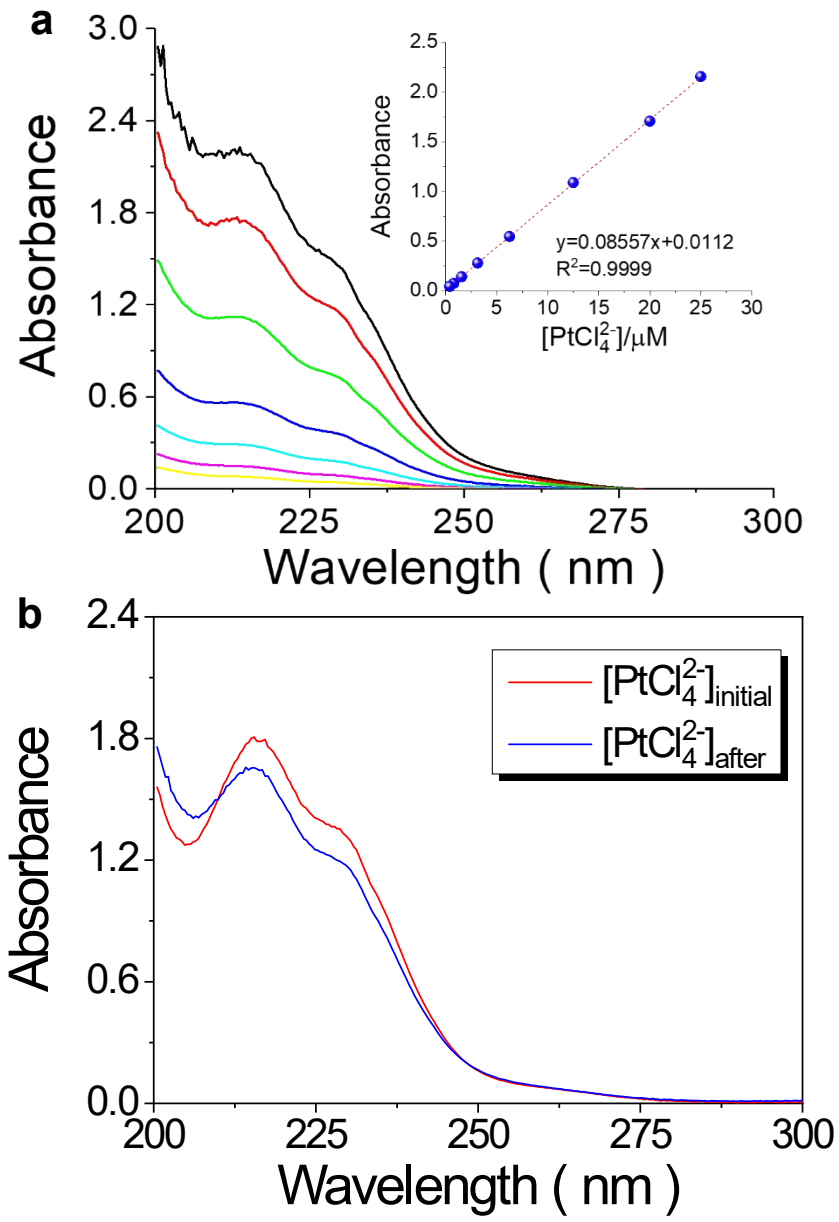

Fig. S3 UV-Vs absorption spectra (a) 200–300 nm recorded in various of $[PtCl_4^{2-}]$. The inset is a calibration curve recorded as the absorbance on $\lambda_{216\,nm}$ vs. $[PtCl_4^{2-}]$; (b) Tracking reduction of absorbance on $\lambda_{216\,nm}$ before and after $PtCl_4^{2-}/TA_i/C$ precipitation in $PtCl_4^{2-}$-containing aqueous solution.

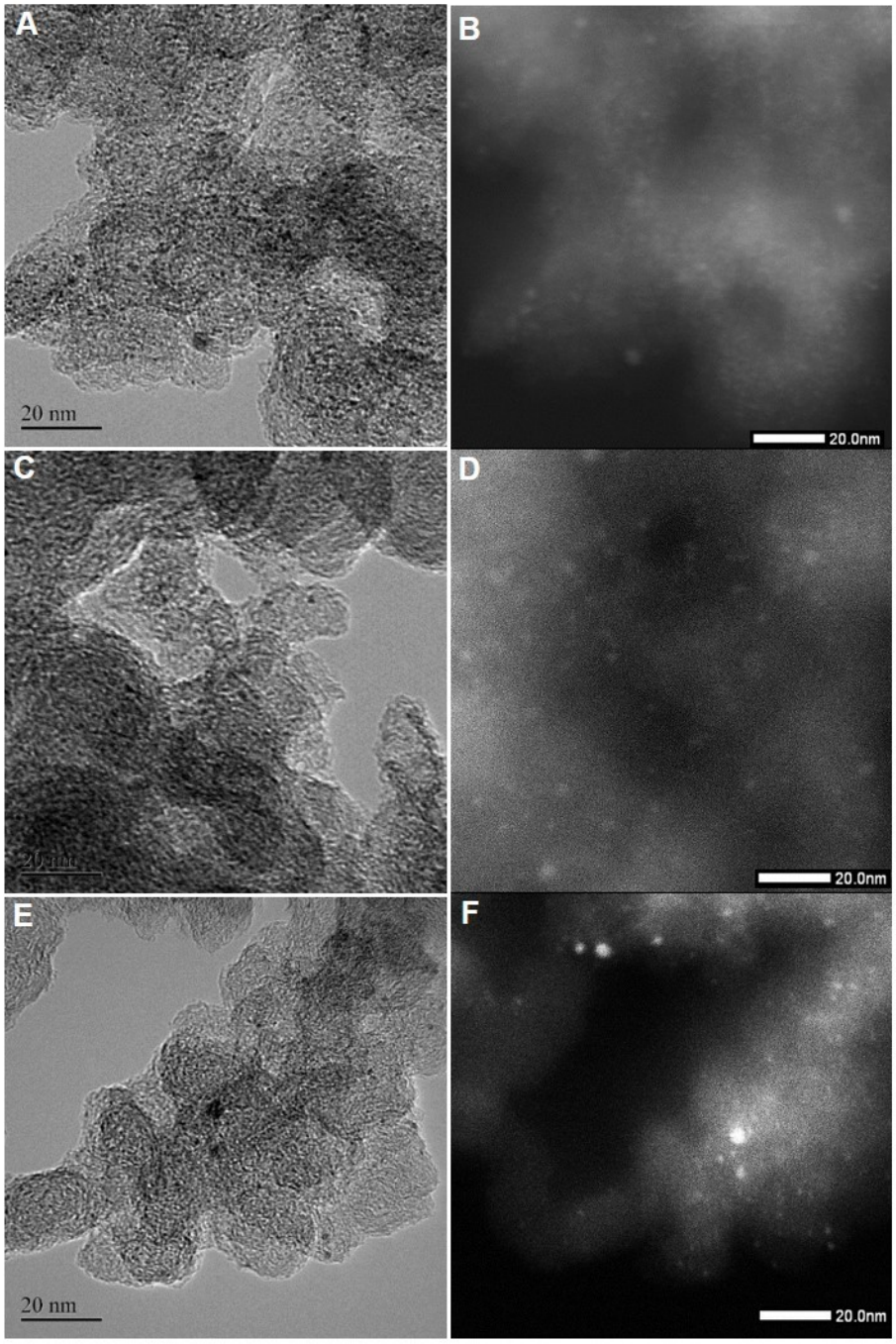

Fig. S4 HR-TEM images of (a) $Pt_c(250)/C$, (c) $Pt_c(300)/C$, and (e) $Pt_c(500)/C$. (b)(d)(f) are corresponding HAADF-STEM images of (a)(c)(e).

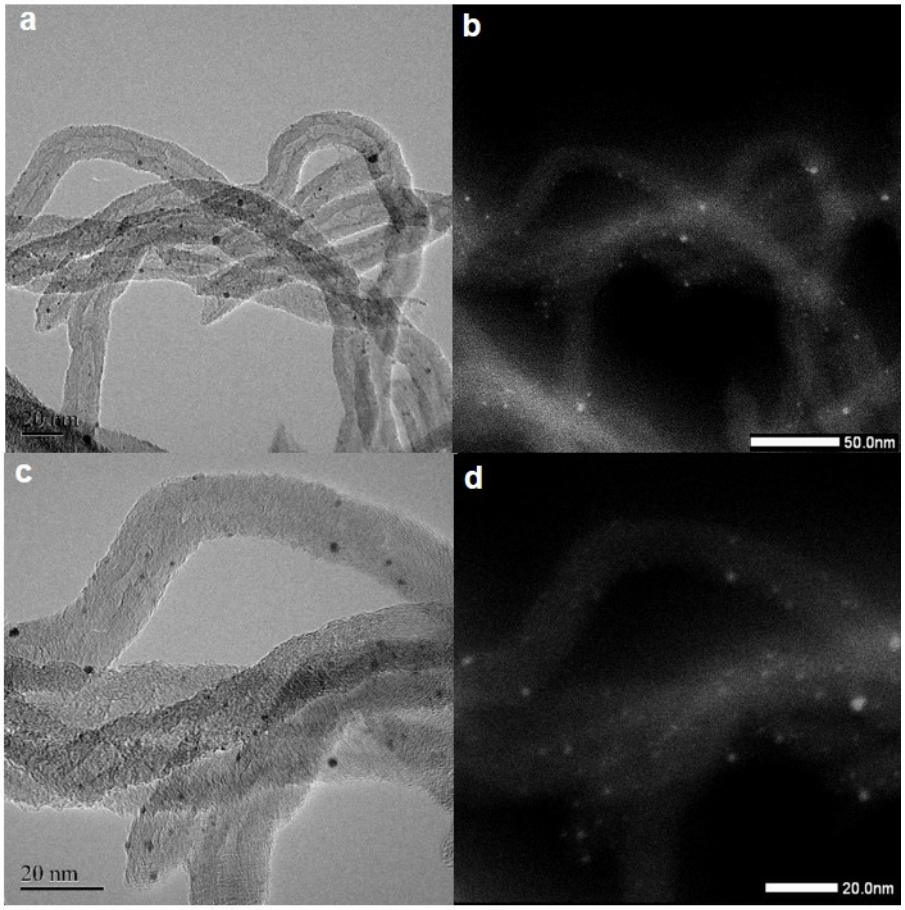

Fig. S5 (a) Low-magnification and (c) high-magnification HR-TEM images of Pt_c formed on the MWCNT. (b)(d) are corresponding HAADF-STEM images of (a)(c).

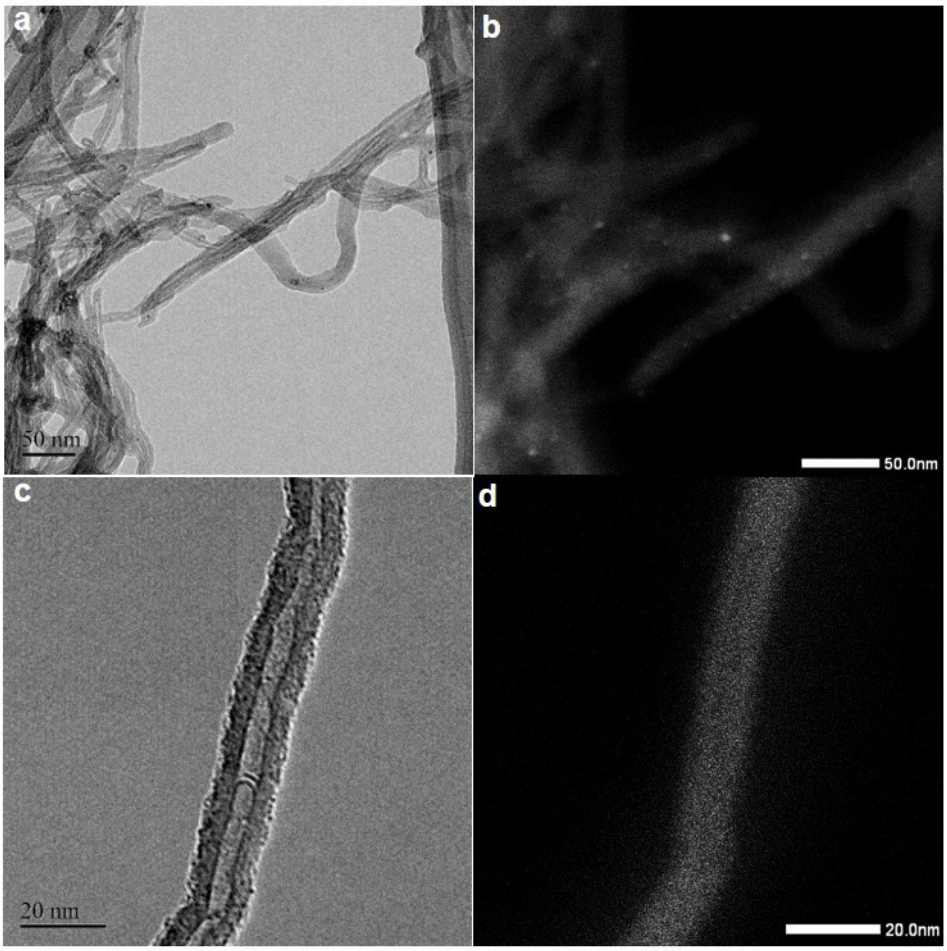

Fig. S6 (a) Low-magnification and (c) high-magnification HR-TEM images of Pt_c formed on the SWCNT. (b)(d) are corresponding HAADF-STEM images of (a)(c).

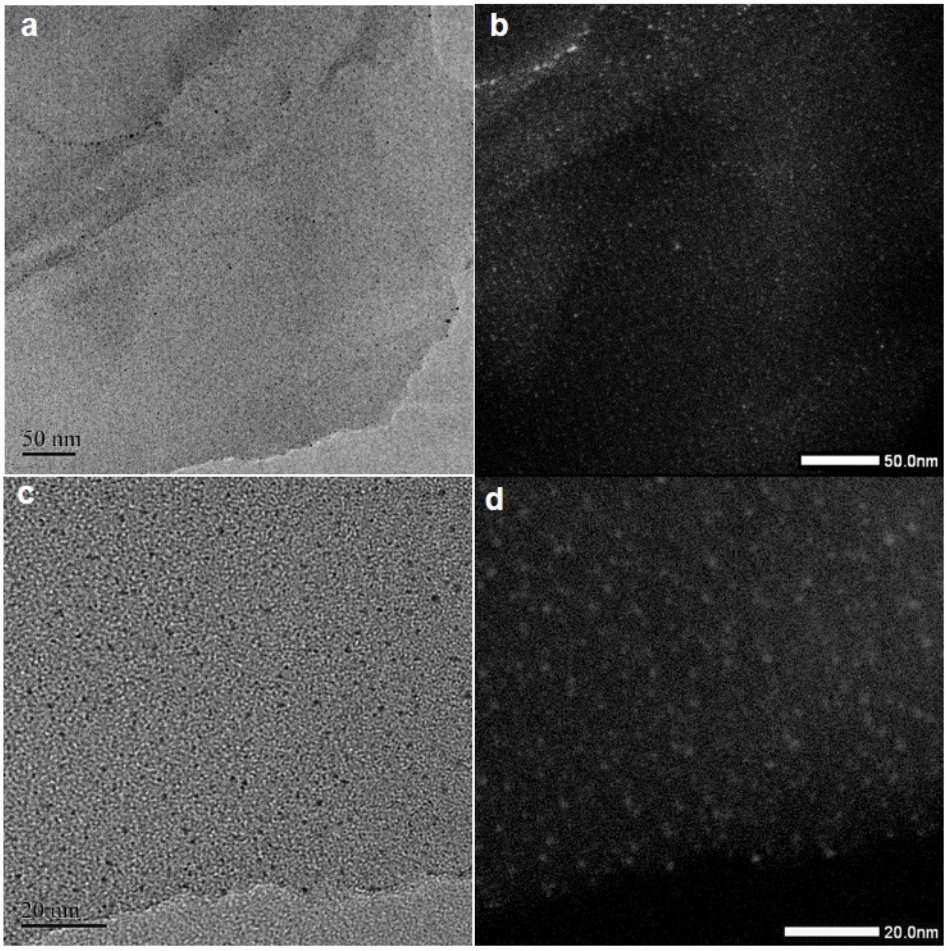

Fig. S7 (a) Low-magnification and (c) high-magnification HR-TEM images of Pt_c formed on the graphene. (b)(d) are corresponding HAADF-STEM images of (a)(c).

S-3 Electrochemical characterization of Pt_c

The anodic charge (Q_{Pt}) of the anodic stripping of Pt_c from Pt/C@GCE was evaluated during anodic CV scanning (Figure 2b). The Pt_c content was evaluated directly from Q_{Pt} with the value of four electrons transferred per Pt atom. This result is consistent with the Pt amounts evaluated by ICP-MS and TGA. A combination of $ECSA_{CO}$ and Q_{Pt} was used to calculate the mean diameter of Pt_c (D_{Ptc}) and the number of Pt_c particles on the electrode (N_{Ptc}).[27, 30] Assuming that the Pt_c on the electrode is distributed uniformly and is spherical in shape, $ECSA_{CO}$ and Q_{Pt} can be calculated using equations (1) and (2), respectively.

$$ECSA_{CO} = \frac{\pi D_{Ptc}^{\ 2}}{2} \times N_{Ptc} \qquad (1)$$

$$Q_{Pt} = \frac{\pi D_{Ptc}^{\ 3} \rho_{Pt}}{6M_{Pt}} \times n \times F \times N_{Ptc} \qquad (2)$$

where n= 4 is the number of electrons transferred for the anodic stripping of Pt, F is the Faraday constant, ρ_{Pt} is the density of Pt (21.09 g cm^{-3}), and M_{Pt} is the atomic mass of Pt. The Q_{Pt}/ECSA ratio for the evaluation of the D_{Ptc} of Pt_c is shown in equation (3). N_{Ptc} can then be obtained from D_{Ptc}.

$$D_{Ptc} = \frac{3M_{Pt}}{4F\rho_{Pt}} \times \frac{Q_{Pt}}{ECSA_{CO}} \qquad (3)$$

We proposed the inter-particle distance (D_{ee}) as a controlling parameter for the thermal stability and HER kinetics of Pt_c(T)/C electrocatalysts. D_{ee} represents the distance between two Pt_cs affected by the control parameters (D_{Ptc}, A_{BET}, and Pt loading). Thus, D_{ee} translates the different control parameters into only one parameter (D_{ee}) and allows the comparison of various Pt/C materials. We assumed that all the Pt_cs exhibit a spherical shape for the calculation of D_{ee}. The particles were monodispersed and homogenously distributed on the carbon support (Figure S8).

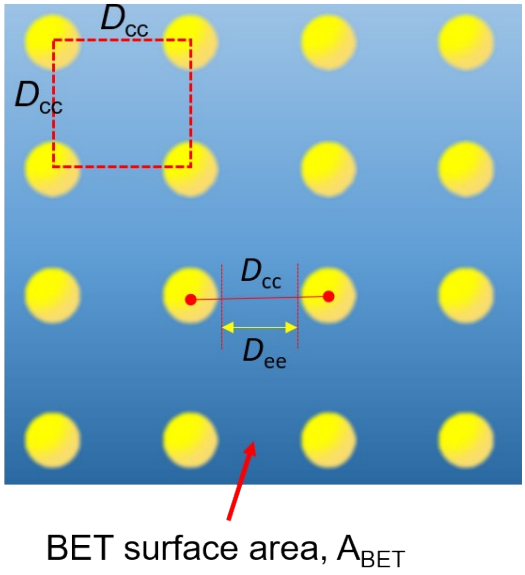

Fig. S8 Evaluation of D_{ee} (edge to edge distance between each Pt_c): D_{cc} (center to center distance between each Pt_c) = $(A_{BET}/N_{Ptc})^{0.5}$; D_{ee} (edge to edge distance between each Pt_c) = D_{cc}-D_{Ptc}=$(A_{BET}/N_{Ptc})^{0.5}$-D_{Ptc}. (Note: N_{Ptc} is the number of Pt_c and A_{BET} is BET surface area of CS)

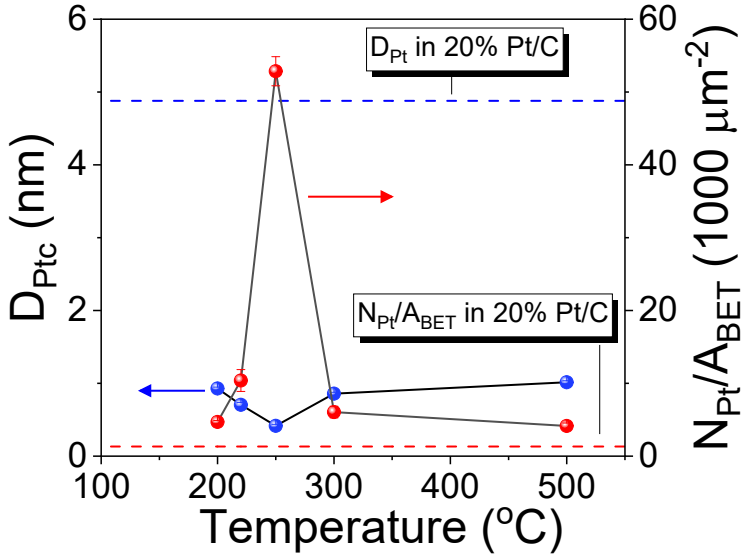

Fig. S9 D_{Ptc} and N_{Pt}/A_{BET} of $Pt_c(T)/C$ vs. thermal treating temperature (red and blue parallel straight lines present D_{Ptc} and N_{Pt}/A_{BET} of Pt_{20}/C).

S-4 XPS of TA/C

XPS was used to investigate the elemental states of TA/C before and after the thermal treatment. In the C 1*s* spectra of TA/C (Figure S10), the TA characteristic peaks at 287.4, 284.1, and 283.2 eV are attributed to C=O, C-O, and C-C (aromatic), respectively.[2] The replacement of the C-C (graphite) by the C-C (aromatic) indicates TA well-modified the surface of C. After thermal treatments at 250 °C and 500 °C thermal treatments under Ar, the C=O and C-O peaks disappeared, but the C-C (aromatic) peak C signal was retained. The above results are consistent with the TGA data (Figure 4a) showing that the inner structure of TA is retained after thermal treatment above 200 °C under inert gas. Additionally, Pt_c did not significantly affect the C 1*s* spectra.

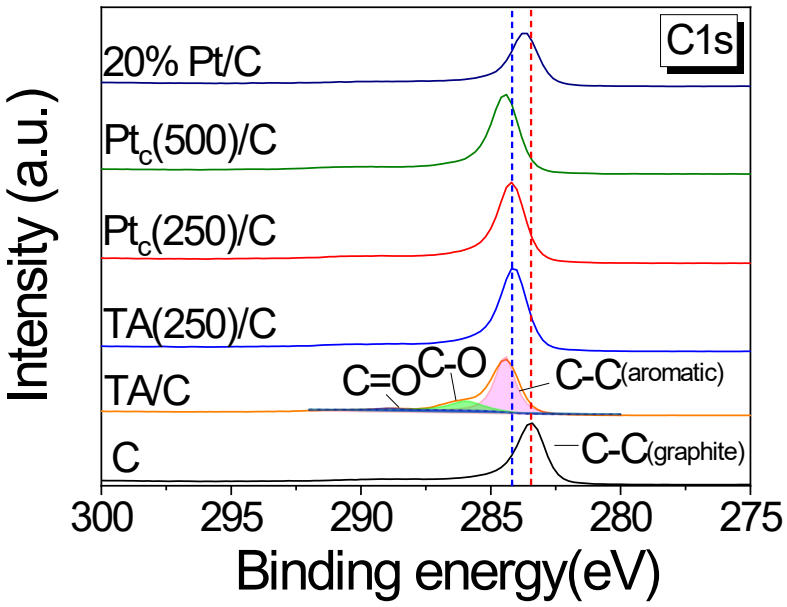

Fig. S10 High-resolution XPS C 1s spectra of Pt_{20}/C, Pt_c(500)/C, Pt_c(250)/C, TA/C before and after (TA(250)/C) thermal treatment at 250°C, and XC-72 (C).

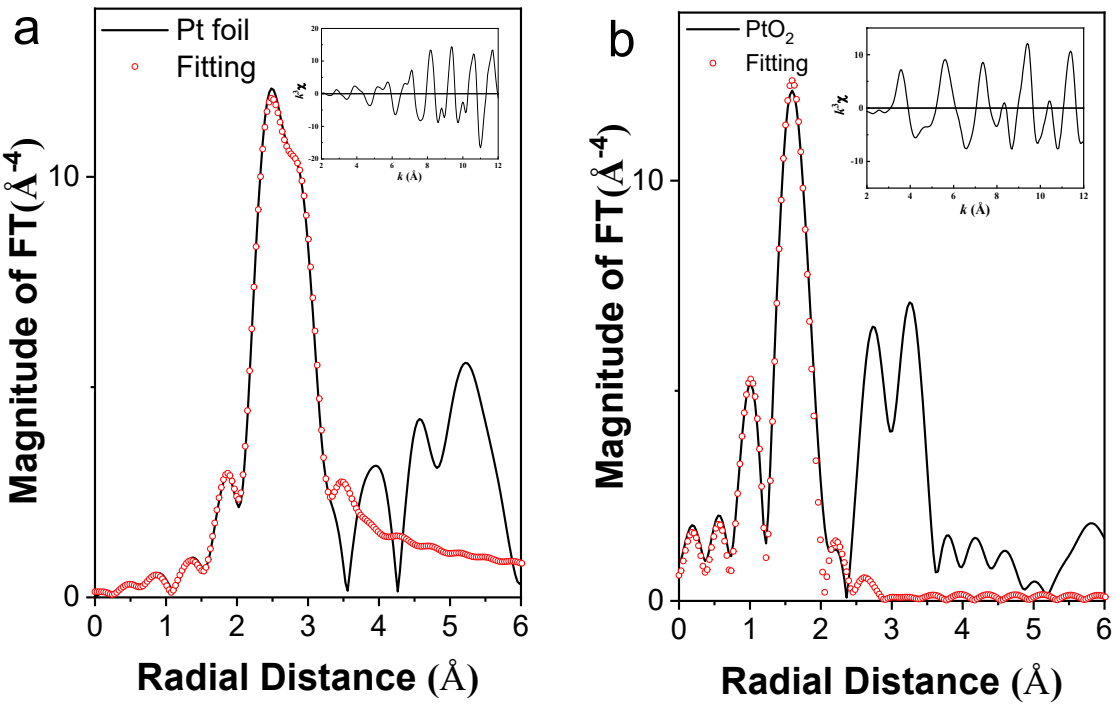

Fig. S11 The FT-EXAFS fitting in R-space for (a) Pt foil and (b) PtO_2. (inset: The spectra in k space).

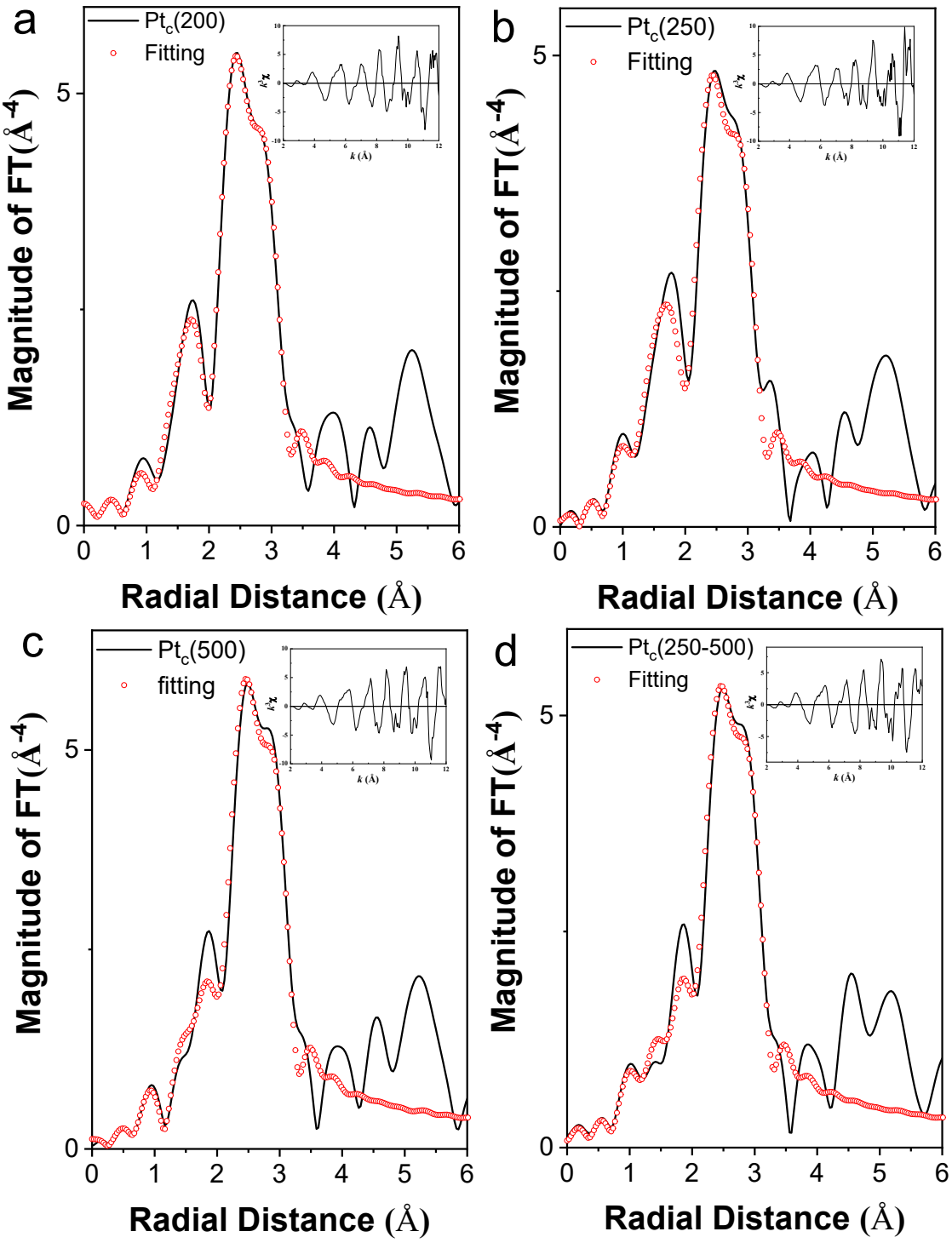

Fig. S12 The FT-EXAFS fitting in R-space for (a) Pt$_c$(200), (b) Pt$_c$(250), (c) Pt$_c$(500), and (d) Pt$_c$(250-500). (inset: The spectra in k space).

Table S1 EXAFS fitting parameters at the Pt L3-edge for various samples

Sample	shell	N[a]	R[b] (Å)	σ^{2} [c] (Å^2)	R_f
Pt foil	Pt-Pt	12	2.76	0.004	0.003
PtO_2	Pt-O	6	2.02	0.002	0.024
Pt_c(200)	Pt-Pt	7.09	2.75	0.006	0.027
	Pt-O	0.98	2.00	0.001	0.027
Pt_c(250)	Pt-Pt	6.65	2.75	0.006	0.034
	Pt-O	1.17	2.00	0.003	0.034
Pt_c(500)	Pt-Pt	8.06	2.75	0.005	0.023
	Pt-O	0.87	2.01	0.003	0.023
Pt_c(250-500)	Pt-Pt	6.95	2.75	0.006	0.032
	Pt-O	1.09	2.00	0.007	0.032

[a]N: coordination number; [b]R: bond distance; [c]σ^2: Debye–Waller factor; R_f: R-factor, is characterizing the goodness of fit. S_o^2 was fixed to 0.77 as determined from Pt foil fitting. Error bounds (accuracies) characterizing the structural parameters obtained by EXAFS data analysis are estimated to be as follows: N, ±20%; R, ±1%; and σ^2, ±20%.

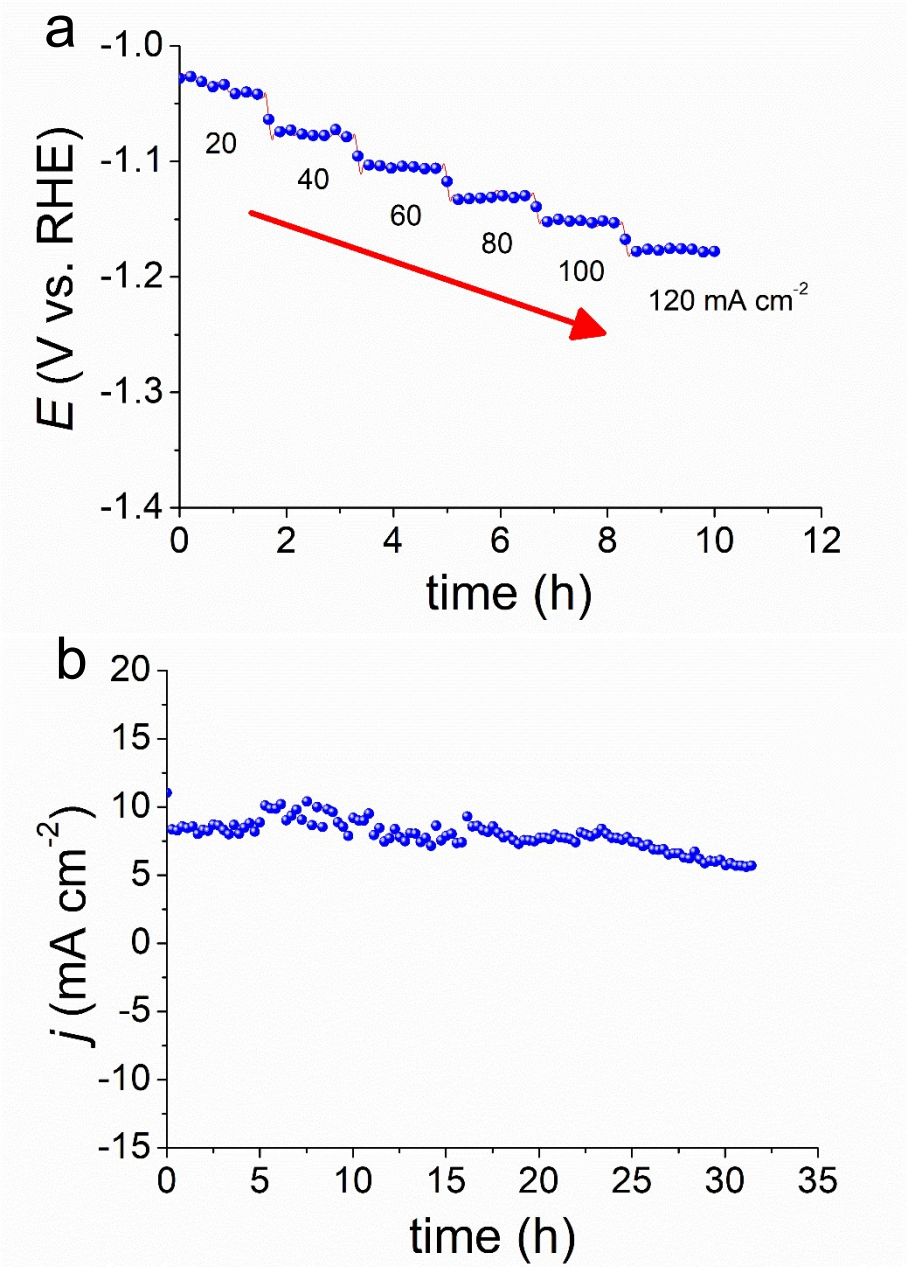

Fig. S13 Long-term stabilities of $Pt_c(250)$: (a) HER chronopotentiometry curves at a series of current densities and (b) the HER chronoamperometry curve at 0.04 V vs. RHE in a 0.5 M H_2SO_{4aq}.

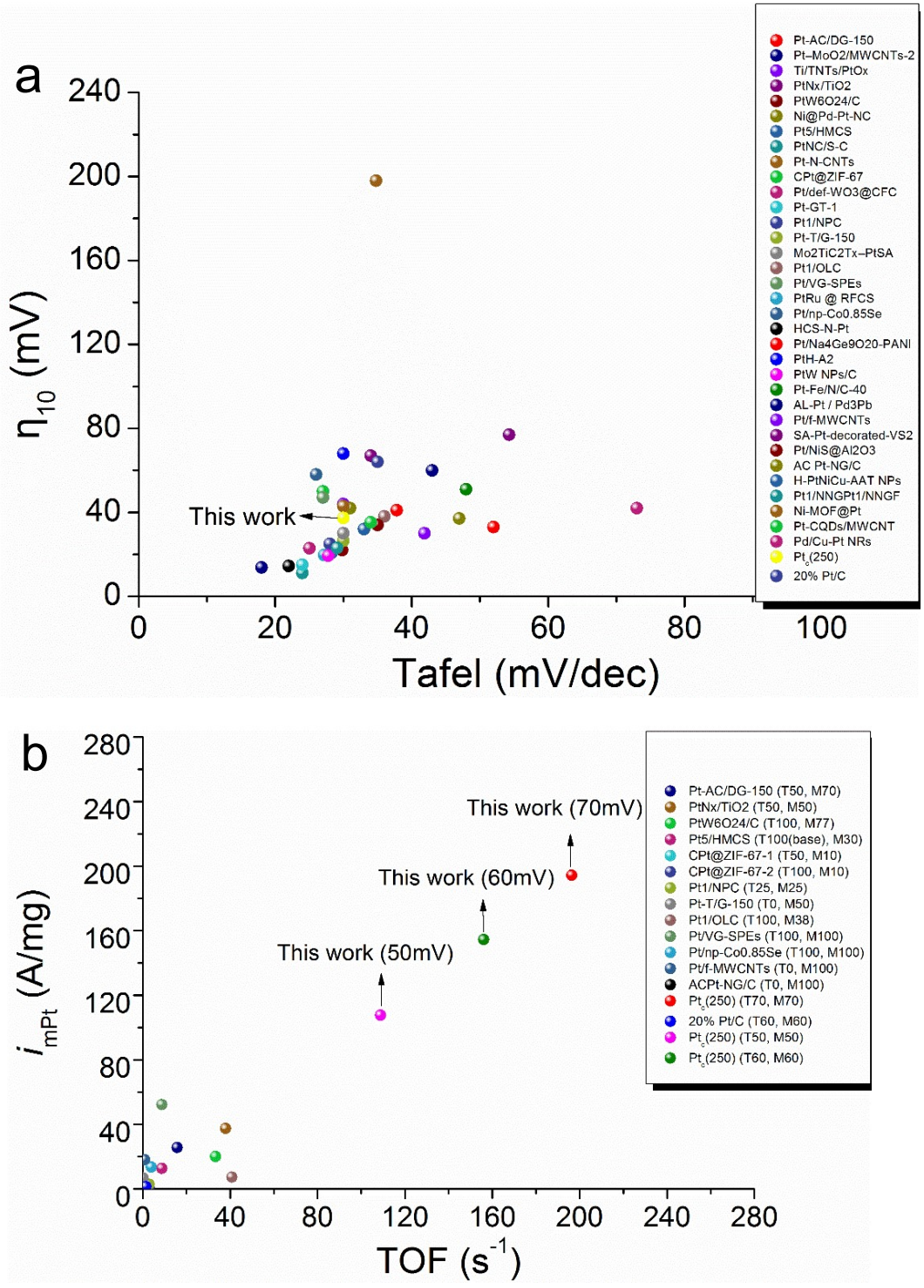

Fig. S14 Comparison of (a) η_{10}/Tafel slope and (b) i_{mPt}/TOF of $Pt_c(250)/C$ with commercial 20% Pt/C and other recently reported Pt containing SAC HER electrocatalysts.

Table S2 HER performance of $Pt_c(250)/C$ and other reported Pt-based catalysts in acidic medium.

Catalyst	η_{10} (mV)	Tafel slopes (mV dec^{-1})	TOF(η) (s^{-1})	j_{mPt} (η) (A mg^{-1})	Refs.
$Pt_C(250)$	37.4	30	108.8 (50mV)	107.7 (50mV)	This work
$Pt_C(250)$	37.4	30	156.1 (60mV)	154.5 (60mV)	This work
$Pt_C(250)$	37.4	30	196.4 (70mV)	194.4 (70mV)	This work
Pt/SWNT-O_3	N/A	107	N/A	N/A	S3
Pt-AC/DG-150	41	37.8	15.7 (50mV)	25.7 (70 mV)	S4
Pt–MoO_2/MWCNTs	60	43	11.5 (100mV)	N/A	S5
Ti/TNTs/PtO x	30	41.9	N/A	0.20 (30 mV)	S6
PtN_x/TiO_2	67	34	38.0 (50mV)	37.5 (50 mV)	S7
PtW_6O_{24}/C	22	29.8	33.4 (100mV)	20.2 (77 mV)	S8
Ni@Pd-Pt NC	37	47	N/A	N/A	S9
Pt5/HMCS	20.7	28.3	8.8 (100mV)	12.8 (30 mV)	S10
PtNC/S-C	11	24	N/A	26.1 (20 mV)	S11
Pt-N-CNTs	198	34.79	0.265 (300mV)	N/A	S12
CPt@ZIF-67	50	27	2.94 (100mV)	0.87 (10 mV)	S13
Pt/def-WO3@CFC	42	73	N/A	1.11 (70 mV)	S14
Pt0.2-TiO_2 Nanowires	N/A	35	N/A	1.18 (50 mV)	S15
Pt-GT-1	15	24	7.22 (66mV)	N/A	S16
Pt1/NPC	25	28	2.93 (25mV)	2.86 (25 mV)	S17
Pt-T/G-150	26.4	30	0.165(0mV)	6.84 (50 mV)	S18
Pt-MoS_2	N/A	44	N/A	N/A	S19
Mo_2TiC_2Tx–PtSA	30	30	N/A	8.3 (77 mV)	S20
Pt1/OLC	38	36	40.8 (100mV)	7.4 (38 mV)	S21
Pt/VG-SPEs	47	27	8.77 (100mV)	52.3 (100 mV)	S22
PtRu @ RFCS	19.7	27.2	4.03 (100mV)	N/A	S23
Pt/np-$Co_{0.85}Se$	58	26	3.93 (100mV)	13.6 (100 mV)	S24
HCS-N-Pt	14.4	22	1.5 (70mV)	N/A	S25
Pt/$Na_4Ge_9O_{20}$-PANI	33	52	N/A	3.0 (0 mV)	S26
PtH-A2	68	30	N/A	N/A	S27
PtW NPs/C	19.4	27.8	N/A	0.6 (20 mV)	S28
CNT/Pt@CdSe-OCPs	N/A	61.3	84.2 (100mV)	166.2 (150 mV)	S29
Pt-Fe/N/C-40	51	48	N/A	1.54 (50 mV)	S30
AL-Pt/Pd_3Pb	13.8	18	N/A	7.83 (50 mV)	S31
Pt/f-MWCNTs	43.9	30	0.921 (0mV)	18.2 (50 mV)	S32
SA-Pt-decorated-VS_2	77	54.27	N/A	22.9 (200 mV)	S33
Pt-GDY2	N/A	46.6	N/A	23.6 (100 mV)	S34
Pt/NiS@Al_2O_3	34	35	N/A	N/A	S35

AC Pt-NG/C	42.03	31	0.093 (0mV)	6.51 (50 mV)	S36
H-PtNiCu-AAT NPs	32	33	N/A	0.977 (90 mV)	S37
3ZIF-67-Pt / RGO	14.3	12.5	N/A	0.193 (90 mV)	S38
LP@PF	N/A	21.3	N/A	12.4 (90 mV)	S39
Pt1/NNGF	23	29.1	N/A	14.6 (50 mV)	S40
Ni-MOF@Pt	43	30	N/A	0.126 (35 mV)	S41
$Pd_{43}Ag_{21}Pt_{36}$	9	19.6	N/A	1.78 (50 mV)	S42
Pt-CQDs/MWCNT	35.3	34	N/A	4.89 (40 mV)	S43
Pt SASs/AG	12	29.33	N/A	22 .4 (50 mV)	S44
Pd/Cu-Pt NRs	22.8	25	N/A	3.00 (50 mV)	S45

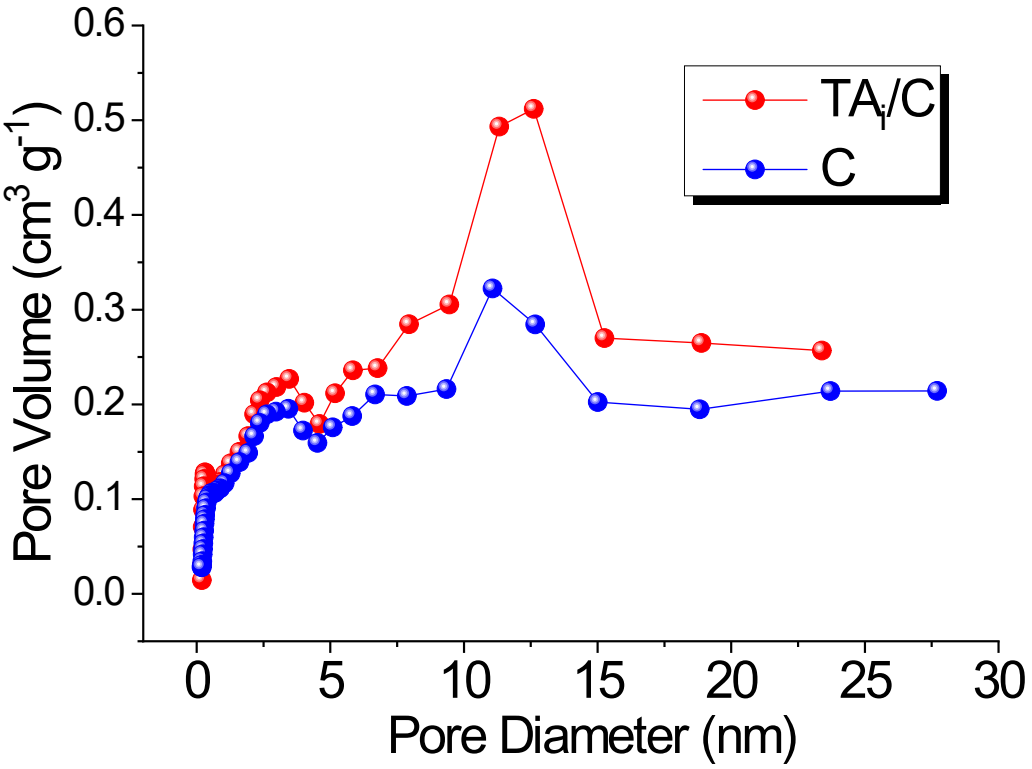

Fig. S15 The pore-size distributions of the XC-72 Vulcan carbon before (C) and after modification of TA_i (TA_i/C) were calculated with the BJH method based on the N_2 adsorption isotherms.

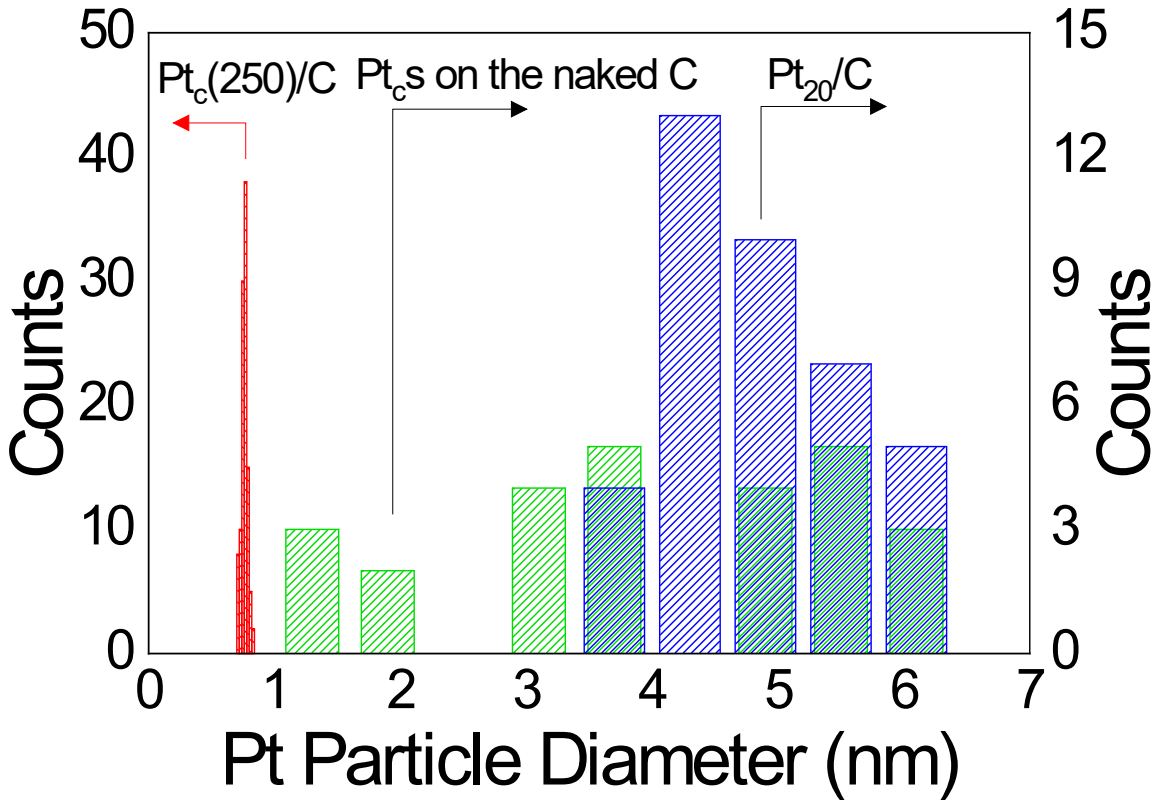

Fig. S16 The histogram presents the Pt particle size distributions of $Pt_c(250)/C$, Pt_cs formed on the naked C, and commercial Pt_{20}/C shown in Fig. 1.

References

1. J. F. Huang and W. Z. Xie, *Chem. Sci.*, 2020, **11**, 6012-6019.
2. A. Chilkoti, B. D. Ratner and D. Briggs, *Chem. Mat.*, 1991, **3**, 51-61.
3. T. Rajala, R. Kronberg, R. Backhouse, M. E. M. Buan, M. Tripathi, A. Zitolo, H. Jiang, K. Laasonen, T. Susi, F. Jaouen and T. Kallio, *Appl. Catal. B-Environ.*, 2020, **265**, 12.
4. Q. Q. Cheng, C. G. Hu, G. L. Wang, Z. Q. Zou, H. Yang and L. M. Dai, *J. Am. Chem. Soc.*, 2020, **142**, 5594-5601.
5. X. Xie, Y. F. Jiang, C. Z. Yuan, N. Jiang, S. J. Zhao, L. Jia and A. W. Xu, *J. Phys. Chem. C*, 2017, **121**, 24979-24986.
6. K. M. AlAqad, T. A. Kandiel and C. Basheer, *ChemCatChem*, 2020, **12**, 5411-5419.
7. X. Cheng, Y. Lu, L. R. Zheng, Y. T. Cui, M. Niibe, T. Tokushima, H. Y. Li, Y. F. Zhang, G. Chen, S. R. Sun and J. J. Zhang, *Nano Energy*, 2020, **73**, 10.
8. F. Y. Yu, Z. L. Lang, L. Y. Yin, K. Feng, Y. J. Xia, H. Q. Tan, H. T. Zhu, J. Zhong, Z. H. Kang and Y. G. Li, *Nat. Commun.*, 2020, **11**, 7.
9. D. Bhalothia, S. P. Wang, S. Lin, C. Yan, K. W. Wang and P. C. Chen, *Appl. Sci.-Basel*, 2020, **10**, 11.
10. X. K. Wan, H. B. Wu, B. Y. Guan, D. Y. Luan and X. W. Lou, *Adv. Mater.*, 2020, **32**, 8.
11. Q. Q. Yan, D. X. Wu, S. Q. Chu, Z. Q. Chen, Y. Lin, M. X. Chen, J. Zhang, X. J. Wu and H. W. Liang, *Nat. Commun.*, 2019, **10**, 9.
12. F. Han, Z. W. Liu, J. Jia, J. Ai, L. Liu, J. L. Liu and Q. D. Wang, *Mater. Chem. Phys.*, 2019, **237**, 9.
13. Y. D. Qin, X. Y. Han, S. Gadipelli, J. Guo, S. J. Wu, L. Q. Kang, J. Callison and Z. X. Guo, *J. Mater. Chem. A*, 2019, **7**, 6543-6551.
14. H. Tian, X. Z. Cui, L. M. Zeng, L. Su, Y. L. Song and J. L. Shi, *J. Mater. Chem. A*, 2019, **7**, 6285-6293.
15. J. J. Gao, P. Du, Q. H. Zhang, X. Shen, F. K. Chiang, Y. R. Wen, X. Lin, X. J. Liu and H. J. Qiu, *Electrochim. Acta*, 2019, **297**, 155-162.
16. J. N. Tiwari, S. Sultan, C. W. Myung, T. Yoon, N. N. Li, M. R. Ha, A. M. Harzandi, H. J. Park, D. Y. Kim, S. S. Chandrasekaran, W. G. Lee, V. Vij, H. J. Kang, T. J. Shin, H. S. Shin, G. Lee, Z. Lee and K. S. Kim, *Nat. Energy*, 2018, **3**, 773-782.
17. T. F. Li, J. J. Liu, Y. Song and F. Wang, *ACS Catal.*, 2018, **8**, 8450-8458.
18. J. P. Ji, Z. H. Li, C. C. Hu, Y. Sha, S. Y. Li, X. H. Gao, S. Y. Zhou, T. Qiu, C. Y. Liu, X. T. Su, Y. Hou, Z. Lin, S. D. Zhou, M. Ling and C. D. Liang, *ACS Appl. Mater. Interfaces*, 2020, **12**, 40204-40212.
19. S. Li, J. K. Lee, S. Zhou, M. Pasta and J. H. Warner, *Chem. Mat.*, 2019, **31**, 387-397.
20. J. Q. Zhang, Y. F. Zhao, X. Guo, C. Chen, C. L. Dong, R. S. Liu, C. P. Han, Y. D. Li, Y. Gogotsi and G. X. Wang, *Nat. Catal.*, 2018, **1**, 985-992.
21. D. B. Li, X. Y. Li, S. M. Chen, H. Yang, C. D. Wang, C. Q. Wu, Y. A. Haleem, S. Duan, J. L. Lu, B. H. Ge, P. M. Ajayan, Y. Luo, J. Jiang and L. Song, *Nat. Energy*, 2019, **4**, 512-518.
22. J. Scremin, I. V. J. dos Santos, J. P. Hughes, A. G. M. Ferrari, E. Valderrama, W. Zheng, X. Z. Zhong, X. Zhao, E. J. R. Sartori, R. D. Crapnell, S. J. Rowley-Neale and C. E. Banks, *Nanoscale*, 2020, **12**, 18214-18224.
23. K. Li, Y. Li, Y. M. Wang, J. J. Ge, C. P. Liu and W. Xing, *Energy Environ. Sci.*, 2018, **11**, 1232-1239.
24. K. Jiang, B. Y. Liu, M. Luo, S. C. Ning, M. Peng, Y. Zhao, Y. R. Lu, T. S. Chan, F. M. F.

de Groot and Y. W. Tan, *Nat. Commun.*, 2019, **10**, 9.
25. X. Shang, Z. Z. Liu, S. S. Lu, B. Dong, J. Q. Chi, J. F. Qin, X. Liu, Y. M. Chai and C. G. Liu, *ACS Appl. Mater. Interfaces*, 2018, **10**, 43561-43569.
26. M. Wang, L. H. Jiang, Q. R. Li and X. X. Zhou, *Int. J. Hydrog. Energy*, 2019, **44**, 31062-31071.
27. E. T. Adesuji, L. E. Khalil-Cruz, M. Videa and M. Sanchez-Dominguez, *Electrochim. Acta*, 2020, **354**, 14.
28. D. Kobayashi, H. Kobayashi, D. S. Wu, S. Okazoe, K. Kusada, T. Yamamoto, T. Toriyama, S. Matsumura, S. Kawaguchi, Y. Kubota, S. M. Aspera, H. Nakanishi, S. Arai and H. Kitagawa, *J. Am. Chem. Soc.*, 2020, **142**, 17250-17254.
29. L. Najafi, S. Bellani, A. Castelli, M. P. Arciniegas, R. Brescia, R. Oropesa-Nunez, B. Martin-Garcia, M. Serri, F. Drago, L. Manna and F. Bonaccorso, *Chem. Mat.*, 2020, **32**, 2420-2429.
30. H. Y. Li, G. L. Wang, F. R. Zhang, L. L. Zou, Z. Q. Zou and H. Yang, *J. Phys. Chem. C*, 2020, **124**, 11760-11766.
31. Y. C. Yao, X. K. Gu, D. S. He, Z. J. Li, W. Liu, Q. Xu, T. Yao, Y. Lin, H. J. Wang, C. M. Zhao, X. Q. Wang, P. Q. Yin, H. Li, X. Hong, S. Q. Wei, W. X. Li, Y. D. Li and Y. E. Wu, *J. Am. Chem. Soc.*, 2019, **141**, 19964-19968.
32. J. P. Ji, Y. P. Zhang, L. B. Tang, C. Y. Liu, X. H. Gao, M. H. Sun, J. C. Zheng, M. Ling, C. D. Liang and Z. Lin, *Nano Energy*, 2019, **63**, 8.
33. J. T. Zhu, L. J. Cai, X. M. Yin, Z. Wang, L. F. Zhang, H. B. Ma, Y. X. Ke, Y. H. Du, S. B. Xi, A. T. S. Wee, Y. Chai and W. J. Zhang, *ACS Nano*, 2020, **14**, 5600-5608.
34. X. P. Yin, H. J. Wang, S. F. Tang, X. L. Lu, M. Shu, R. Si and T. B. Lu, *Angew. Chem.-Int. Edit.*, 2018, **57**, 9382-9386.
35. Y. Y. Feng, Y. X. Guan, H. J. Zhang, Z. Y. Huang, J. Li, Z. Q. Jiang, X. Gu and Y. Wang, *J. Mater. Chem. A*, 2018, **6**, 11783-11789.
36. M. H. Sun, J. P. Ji, M. Y. Hu, M. Y. Weng, Y. P. Zhang, H. S. Yu, J. J. Tang, J. C. Zheng, Z. Jiang, F. Pan, C. D. Liang and Z. Lin, *ACS Catal.*, 2019, **9**, 8213-8223.
37. D. F. Wu, W. Zhang, A. J. Lin and D. J. Cheng, *ACS Appl. Mater. Interfaces*, 2020, **12**, 9600-9608.
38. W. Wu, Z. Y. Zhang, Z. Lei, X. Y. Wang, Y. Y. Tan, N. C. Cheng and X. L. Sun, *ACS Appl. Mater. Interfaces*, 2020, **12**, 10359-10368.
39. L. Chong, J. G. Wen, J. Kubal, F. G. Sen, J. X. Zou, J. Greeley, M. Chan, H. Barkholtz, W. J. Ding and D. J. Liu, *Science*, 2018, **362**, 1276-+.
40. J. S. Xu, R. Li, R. G. Zeng, X. Y. Yan, Q. K. Zhao, J. W. Ba, W. H. Luo and D. Q. Meng, *ACS Appl. Mater. Interfaces*, 2020, **12**, 38106-38112.
41. K. Rui, G. Q. Zhao, M. M. Lao, P. X. Cui, X. S. Zheng, X. B. Zheng, J. X. Zhu, W. Huang, S. X. Doug and W. P. Sun, *Nano Lett.*, 2019, **19**, 8447-8453.
42. W. Y. Lu, X. Y. Xia, X. X. Wei, M. M. Li, M. Zeng, J. Guo and S. Cheng, *ACS Appl. Mater. Interfaces*, 2020, **12**, 21569-21578.
43. H. Xiao, S. F. Xue, J. J. Zhang, M. Zhao, J. C. Ma, S. Chen, Z. F. Zheng, J. F. Jia and H. S. Wu, *Chem. Eng. J.*, 2021, **408**, 10.
44. S. H. Ye, F. Y. Luo, Q. L. Zhang, P. Y. Zhang, T. T. Xu, Q. Wang, D. S. He, L. C. Guo, Y. Zhang, C. X. He, X. P. Ouyang, M. Gu, J. H. Liu and X. L. Sun, *Energy Environ. Sci.*, 2019, **12**, 1000-1007.
45. T. T. Chao, X. Luo, W. X. Chen, B. Jiang, J. J. Ge, Y. Lin, G. Wu, X. Q. Wang, Y. M. Hu,

Z. B. Zhuang, Y. E. Wu, X. Hong and Y. D. Li, *Angew. Chem.-Int. Edit.*, 2017, **56**, 16047-16051.